Journal of Membrane Science 635 (2021) 119525

Contents lists available at ScienceDirect

Journal of Membrane Science

journal homepage: www.elsevier.com/locate/memsci

Anion exchange membranes with twisted poly(terphenylene) backbone: Effect of the N-cyclic cations

Xiuqin Wang [a], Chenxiao Lin [b], Yang Gao [c], Rob G.H. Lammertink [a,*]

[a] Soft Matter, Fluidics and Interfaces, Faculty of Science and Technology, MESA+ Institute for Nanotechnology, University of Twente, Enschede, 7522, NB, the Netherlands
[b] Department for Electrochemical Energy Storage, Helmholtz-Zentrum Berlin für Materialien und Energie, Hahn-Meitner-Platz, Berlin, 14109, Germany
[c] College of Materials Science and Engineering, Hunan University, Changsha, 410082, China

ARTICLE INFO

Keywords:
N-cyclic cations
Structure-property relationship
Twisted ether-bond free backbone
Anion exchange membrane

ABSTRACT

In order to investigate the relationship towards the cationic structures and ion exchange membrane performance, three kinds of twisted poly(terphenylene)-based anion exchange membranes (AEMs) with N-cyclic cations were prepared via facile Friedel-Crafts type polycondensation and quaternization. The steric hindrance of the N-cyclic cations is gradually increased from the small piperidinium to the sterically protected N-spirocyclic quaternary ammonium (QA). The twisted poly(terphenylene)s backbone promotes the self-assembly of the polymer chain and forms a microphase separated morphology, resulting in a highest conductivity of 68.7 mS cm^{-1} (80 °C) for the polymer tethered with piperidinium groups (m-TPNPiQA). The relative conductivity (conductivity/swelling ratio) of m-TPNPiQA is even higher than that of the commercial Fumapem FAA-3-50 membrane. Increasing the size of the QA is helpful to constrain water absorption and related swelling but has a negative effect on the chemical stability. β-Hofmann elimination degradation is observed for all of the AEMs during a stability test by ^{1}H NMR analysis. The m-TPNPiQA demonstrates less than 6% ionic exchange capacity loss after 240 h in 5 M NaOH solution at 80 °C. The results demonstrated that the membrane performance is associated well with the features of the cationic groups. A high performance AEM can be achieved by grafting appropriate cations onto aryl ether-free backbone.

1. Introduction

Developing high-efficiency energy conversion processes, including alkaline fuel cells and water electrolysis, are considered promising approaches to address challenges regarding sustainable energy and the energy transition. Anion exchange membrane fuel cells (AEMFCs) have earned increasing attention due to their advantages over proton exchange membrane fuel cells, including faster reaction kinetics and the usage of non-previous metal (Ag, Co, etc.) catalysts [1,2]. As the critical component of AEMFCs, the anion exchange membranes (AEMs) function as a separator to separate anode and cathode while conducting hydroxide ions. The low hydroxide conductivity and poor chemical stability of the AEMs are the current major challenges for their application in AEMFCs [3–5].

To address these issues, a variety of polymers, such as polysulfone [6], poly (phenylene oxide)s [7], polybenzimidazole [8], poly (arylene ether)s [9], poly(styrene)s [10], poly(olefin)s [11], etc. with tethered cationic groups have been developed as novel AEM materials for alkaline fuel cell applications. Traditional quaternary ammonium (QA), *e.g.*, benzyl trimethylammonium (BTMA), is the most common used cationic groups due to its simplicity and low cost. However, the BTMA groups are likely to degrade under alkaline condition at elevated temperature because of the nucleophilicity and basicity of OH^- ions [12]. Many efforts have been attempted to improve the stability problem of the cations: 1) modification of QA groups with strong electron donors or bulky steric hindrance [9,13] and 2) development alternative cations such as imidazolium [14,15], sulfonium [16], phosphonium [17] and metal-based cations [18]. Recently, N-cyclic QA cations (piperidinium and N-spirocyclic QA) have attracted more interest [10,13,19–21]. As noted by Jannasch et al., N-spirocyclic QA functionalized polyelectrolytes showed no degradation during 1800 h in 1 M KOD/D_2O at 80 °C since the geometrical constraint of the ring structure increases the transition state energy of the degradation reaction which results in excellent stability under harsh alkaline conditions [21]. Besides, poly

* Corresponding author.
E-mail address: R.G.H.Lammertink@utwente.nl (R.G.H. Lammertink).

https://doi.org/10.1016/j.memsci.2021.119525
Received 7 April 2021; Received in revised form 31 May 2021; Accepted 9 June 2021
Available online 17 June 2021

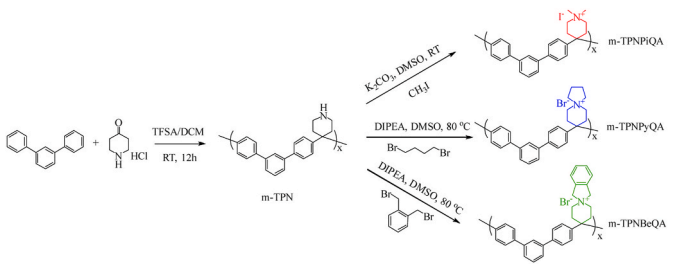

Scheme 1. Synthetic routes for the cationic polymers: m-TPNPiQA, m-TPNPyQA and m-TPNBeQA.

(arylene piperidinium)-based AEMs showed only 5% ionic loss during 15 days in 2 M aq. NaOH at 90 °C [22]. However, it should be emphasized that the alkaline stability of the N-cyclic QA cations-based AEMs could be different depending on the chemical structure of both the cationic group and the polymer backbone. For example, when the N-spirocyclic QA was attached to the poly (arylene ether sulfone) backbone, the AEMs degraded heavily after 7 days in 1 M NaOH solution at 60 °C [23]. That means despite the tremendous advance of N-cyclic QA based AEMs regarding alkaline stability, the cyclic QA cations still potentially degrade via Hofmann elimination under the attack of OH^- due to the existence of β-H in the cationic groups [24]. Thus, the systematical investigation of their relation between the chemical structure of backbone and cationic groups and overall membrane performance is urgently needed.

In order to meet the requirements for practical application, the low conductivity problem of the current AEMs needs to be solved. AEMs with side-chain, block structure and high-density cations were developed to fabricate microphase separated morphologies which seems to be essential for constructing "high-ways" for ion conduction [4,25–28]. The ionic conductivity of these AEMs could be higher than 100 mS cm^{-1}. However, the preparation routes for these AEMs with tailored structures were multistep and complex, limiting their applications in AEMFCs [5]. The aryl ether bond-containing backbones in these AEMs are sensitive to scission reaction and may eventually result in mechanical damage of the AEMs [4,29]. Thus, the use of ether-bond free backbones, such as polystyrene [10], polybenzimidazole [8] and poly(aryl piperidinium) [30] is investigated to further improve the performance of the AEMs. Wang et al. reported a family of novel AEMs with rigid ether-bond free aryl backbone incorporating N-cyclic QA cations [30]. No detectable change in the chemical structure was observed in the ^{1}H NMR spectra after treating the membranes with 1 M KOH at 100 °C for 2000 h. The backbone structure (biphenyl or para-terphenyl) limits the polymer flexibility which seems to be critical for constructing microphase separated structures and forming high-speed ionic channels in the membranes [31]. In contrast, a twisted meta-terphenyl based backbone enables the folding of polymer chain, forming a compact polymer structure and promoting self-assembly of the ionic groups [31]. This could guide the molecular design of polymer materials with improved ionic conductivity and alkaline stability.

Cationic group characteristics such as size, stiffness, hydrophobicity and electron effects will influence the interaction with the backbone. A fundamental understanding regarding the role of N-cyclic cationic groups on the overall membrane performance is important. According to the literature, N-cyclic QAs provide exceptional alkaline stability [13]. To date, only a few studies explore the membrane performance of N-cyclic QA linked to a polymer backbone [10,32,33]. Pham et al. reported the poly(biphenyl piperidine)s AEMs with different N-spirocyclic QA groups [20]. Wang et al. also prepared poly(biphenyl piperidine) AEMs with spirocyclic cationic side chain [34]. However, how the structure of N-cyclic cation affects the overall membrane performance is still unclear.

Here, a series of meta-poly(terphenylene) based AEMs having N-cyclic QA cations with various steric hindrance were prepared via simple polymerization and quaternization (Scheme 1). The steric hindrance of the cations was gradually increased from simple piperidinium to sterically protected N-spirocyclic QA. Poly(terphenylene) was chosen as the polymer backbone due to its ether-bond free structure and self-assembly ability. Twisted meta-terphenyl was selected since AEMs with a twisted backbone (*e.g.* m-triphenyl unit) can form clear microphase separation structures [31]. By the incorporation of the twisted poly (terphenylene) backbone with various N-cyclic cations the influence of cations on the properties of AEMs, including the micro-morphology, water uptake, swelling ratio, ionic conductivity, alkaline stability, thermal stability, etc., were systematically investigated. The results of this study could provide guidance for the molecular design of cations to improve the performance of the AEMs.

2. Experimental

2.1. Materials

m-terphenyl (99%, TCI), 4-piperidone monohydrate hydrochloride (PMH, 98%, Sigma-Aldrich), trifluoromethanesulfonic acid (TFSA, >98%, TCI), trifluoracetic acid (TFA, analytical standard, TCI), potassium carbonate (K_2CO_3, 99%, Sigma-Aldrich), iodomethane (MeI, 99%, Sigma-Aldrich), N,N-diisopropylethylamine (DIPEA, >99%, TCI), 1,4-dibromobutane (99%, Sigma-Aldrich), α,α′-dibromo-o-xylene (97%, Sigma-Aldrich), deuterated dimethyl sulfoxide (DMSO-d_6, 99.96 atom % D, Sigma-Aldrich), diethyl ether (reagent grade, Sigma-Aldrich), ethanol (reagent grade, Sigma-Aldrich) and dimethyl sulfoxide (DMSO, ACS reagent, Sigma-Aldrich) were all used as received. Dichloromethane (DCM, reagent grade, Sigma-Aldrich) was dried by molecular sieve (0.4 nm) before use. Deionized (DI) water was used for membranes treatment and measurements throughout this work. Fumapem FAA-3-50 membrane with a thickness of 50 μm was purchased from Fumatech company (Germany).

2.2. Friedel-crafts type polycondensation of the precursor poly(terphenyl)

The precursor poly(terphenyl) (m-TPN) was synthesized through Friedel-Crafts type polycondensation. m-triphenyl (2.30 g, 1 eq.) and PMH (1.49 g, 1.1 eq.) were dissolved in DCM (50 mL) in a 250 mL flask under stirring and cooled to 0 °C using an ice bath. Then a small amount of TFA (0.78 mL, 1 eq.) and TFSA (8.8 mL, 10 eq.) were added dropwise into the reaction mixture. The reaction was carried out for about 12 h until the viscosity of the solution dramatically increased. The final highly viscous reaction mixture was poured into DI water, resulting in the formation of large amounts of precipitates. Then the precipitates were thoroughly washed with DI water and dried under vacuum at room temperature for 24 h, yielding light-yellow powder (m-TPN) (2.66 g, yield: 84%).

2.3. Quaternizations of m-TPN

m-TPNPiQA, m-TPNPyQA and m-TPNBeQA polymers were obtained via the following steps: To a 100 mL one-neck round bottom flask was added m-TPN (1.0 g, 1 eq.), K_2CO_3 (1.2 g, 3eq.), DMSO (40 mL) and MeI (0.9 mL, 5eq.). The reaction vessel was covered by aluminum foil to prevent light-induced degradation of MeI and stirred at room temperature for 24 h. The resulting solution was precipitated in diethyl ether and washed repeatedly with diethyl ether and ethanol water to remove the impurities. Finally, the resulting products were dried under vacuum overnight to yield light-yellow m-TPNPiQA polymer.

m-TPNPyQA was prepared by cyclo-quaternization using DIPEA as catalyst. The reaction solution in a 100 mL two-neck round bottom flask was made up of m-TPN precursor (1.0 g, 1 eq.), 1,4-dibromopentane (0.40 mL, 1.2 eq.), DIPEA (2.5 mL, 5 eq.) and DMSO (40 mL). The reaction vessel was kept at 80 °C under vigorous stirring for 24 h. After

cooling to room temperature, the resulting solution was precipitated in a mixture of diethyl ether and ethanol solution. Finally, the precipitates were washed and dried under vacuum yielding a red brown powder (m-TPNPyQA).

m-TPNBeQA was synthesized as the same procedure as m-TPNPyQA. Among this, 1,4-dibromopentane was replaced by α, α′-dibromo-o-xylene (0.92 g, 1.2 eq.). The final polymer was obtained as a light brown powder.

2.4. Membranes preparation

AEMs were prepared by 5 wt% solutions casting of the functionalized polymers in DMSO. The typical procedure for membrane preparation is described as follows. 0.25 g of functionalized polymer (m-TPNPiQA, m-TPNPyQA or m-TPNBeQA) was dissolved in DMSO (5 mL) to obtain a homogeneous solution. The solution was filtrated through a Teflon syringe filter (Millex LS, 0.45 μm), and poured into a glass dish (50 × 50 mm), then placed in a ventilated casting oven at 85 °C for at least 24 h. Afterward, the membranes were thoroughly washed with DI water and stored before measurements. The membrane thickness was approximately 50 μm.

2.5. Characterization and measurements

^{1}H NMR. The chemical structures of polymers were confirmed by a Bruker ASCEND™ 400 spectrometer using DMSO-d_6 as the solvent and tetramethyl silane (TMS) as an internal reference.

Gel permeation chromatography (GPC). The number and weight average molecular weight values (M_n and M_w) of the m-TPN precursor were evaluated using HPLC-grade DMF as an eluent at 35 °C in a size-exclusion chromatography system (waters1525 & Agilent PL-GPC220) equipped with three PLgel 3 μm MIXED-E columns and a refractive index detector (Viscotek TDA). Standard polystyrene samples were used for the calibration. Before measurement, a certain amount (3 mg) of dry polymer was first dissolved in 3 mL of DMF solution and filtered through a Teflon filter with the pore size 0.45 μm.

Thermal stability (TGA). The thermal decomposition behaviors of the polymer precursor and functionalized polymer were studied by thermogravimetric analysis using a TA Instruments (PerkinElmer TGA 4000). Prior to analysis, the samples were preheated to 120 °C in the TGA machine to remove traces of absorbed water and any solvent residues. All measurements were performed from 30 to 800 °C at a heating rate of 10 °C min^{-1} under a nitrogen atmosphere.

Differential scanning calorimetry (DSC). The glass transition temperatures (T_g) of each polymer membranes were studied on a STA449F3 thermogravimetric analyzer (NETZSCH, Germany) under the protection of nitrogen with a heating rate of 10 °C min^{-1}.

Ion exchange capacity (IEC). The IEC_{NMR} values of the AEMs were achieved from the NMR spectra of the polymers. The IEC_{titr} values were determined by titration procedures in 805 Dosimat-Metrohm AG. The Br^- or I^- anion (Br^-/I^-) in the AEMs (around 0.1 g) were exchanged with Cl^- anion by treating in a 2 M NaCl at room temperature for 48 h. Then, the membrane samples were washed thoroughly with DI water and immersed in DI water for 48 h to remove residual NaCl. The resulting samples were stored in 2 M aq. $NaNO_3$ (80 mL) under stirring at least 48 h for transfer counter-ions Cl^- into NO_3^- form. Subsequently, the resulting solutions was titrated with a 0.1 M aq. $AgNO_3$ using a silver electrode. Finally, the membrane samples were washed with DI water and dried under vacuum for at least 48 h before measuring their dry weights. The measurements were repeated 3 times to get the average value of IEC_{titr} (meq g^{-1}).

$$IEC_{\text{titr}} = \frac{V_{AgNO_3} \times C_{AgNO_3}}{m_{dry}} \tag{1}$$

The IEC_{OH^-} of the AEMs in the OH^- form was calculated from the IEC.

$$IEC_{OH^-} = \frac{IEC}{1 - \frac{IEC(M_{Cl^-} - M_{OH^-})}{1000}} = \frac{IEC}{1 - 0.01845 \times IEC} \tag{2}$$

The obtained IEC from ^{1}H NMR spectroscopy was calculated by comparing the integral area between protons from the benzene rings and protons from the –CH_2- groups.

Water uptake (WU) and swelling ratio (SR). Square AEMs in Br^-/I^- form (1 × 2 cm^2) were cut. The AEMs in the Br^-/I^- form were transformed into the hydroxide form (OH^-) by immersing the membranes in 1 M aq. NaOH solution for at least 48 h and subsequent washing with DI water. Then the AEMs were equilibrated in DI water for 6 h at 20, 40, 60 and 80 °C, respectively. After removing residual water from the surface of the membranes, the wet weight (m_{wet}, g) and the wet length (L_{wet}, cm) of the AEMs were measured immediately. Subsequently, the dry weight (m_{dry}, g) and dry length (L_{dry}, cm) of membrane samples were obtained after drying the membranes in a vacuum oven at 80 °C to constant mass. The measurements of WU and SR were repeated at least three times to obtain average values. The WU (%) and SR (%) of the membranes can be calculated by the following equation:

$$WU = \frac{m_{wet} - m_{dry}}{m_{dry}} \times 100\% \tag{3}$$

$$SR = \frac{L_{wet} - L_{dry}}{L_{dry}} \times 100\% \tag{4}$$

The hydration number (λ), which is defined as the average number of water molecules per cationic group, was calculated as:

$$\lambda = \frac{WU(\%) \times 10}{IEC \times 18} \tag{5}$$

Static Contact Angle Measurement. The surface hydrophilicity of membrane samples was measured using a contact angle analyzer (OCA 20, Data Physics Instruments GmbH, Germany). For the sessile drop technique, the membranes were taped onto a flat glass slide, 2 μL of DI water was dropped from a micro syringe with a stainless-steel needle onto the membrane's surface at room temperature. The contact angle was determined as the angle between the solid surface and a tangent to the curved surface of the drop within 5 s.

Hydroxide conductivity. The in-plane OH^- conductivity of the AEMs in the fully hydrated state was measured by electrochemical impedance spectroscopy (EIS). The membrane samples in hydroxide form were cut into a 1 × 2 cm rectangles and kept in degassed DI water prior to any measurements to avoid carbonate formation. During the measurements, the membranes were sandwiched in a home-made two-electrode device and placed in a sealed cell. The resistance (R, Ω) of the membrane sample was recorded using an Autolab electrochemical workstation at frequencies ranging from 1 to 10^6 Hz. The thickness of membrane samples was measured by a spiral micrometer. The effective area (cross-sectional area) of the membrane was recorded as A (cm^2). The hydroxide conductivity (σ, mS cm^{-1}) was tested with a temperature range of 20–80 °C at 100% humidity. The measurements were repeated at least three times to obtain an average value. The conductivity can be calculated as follow:

$$\sigma = \frac{L}{AR} \tag{6}$$

where L (cm) is the distance between two electrodes.

Scanning electron microscope (SEM). A field emission SEM (JSM-6010LA) was employed to observe the surface morphology of the membranes. Before observation, the membranes were dried at 30 °C for 12 h and coated with an ultrathin platinum layer to improve the electroconductivity.

Transmission electron microscopy (TEM). TEM images of AEMs were obtained on a JEOL JEM-2100 transmission electron microscope operating at the voltage of 200 kV. Prior to the TEM investigations, the membrane samples were soaking in 0.5 M aq. Na_2WO_3 solution for 48 h

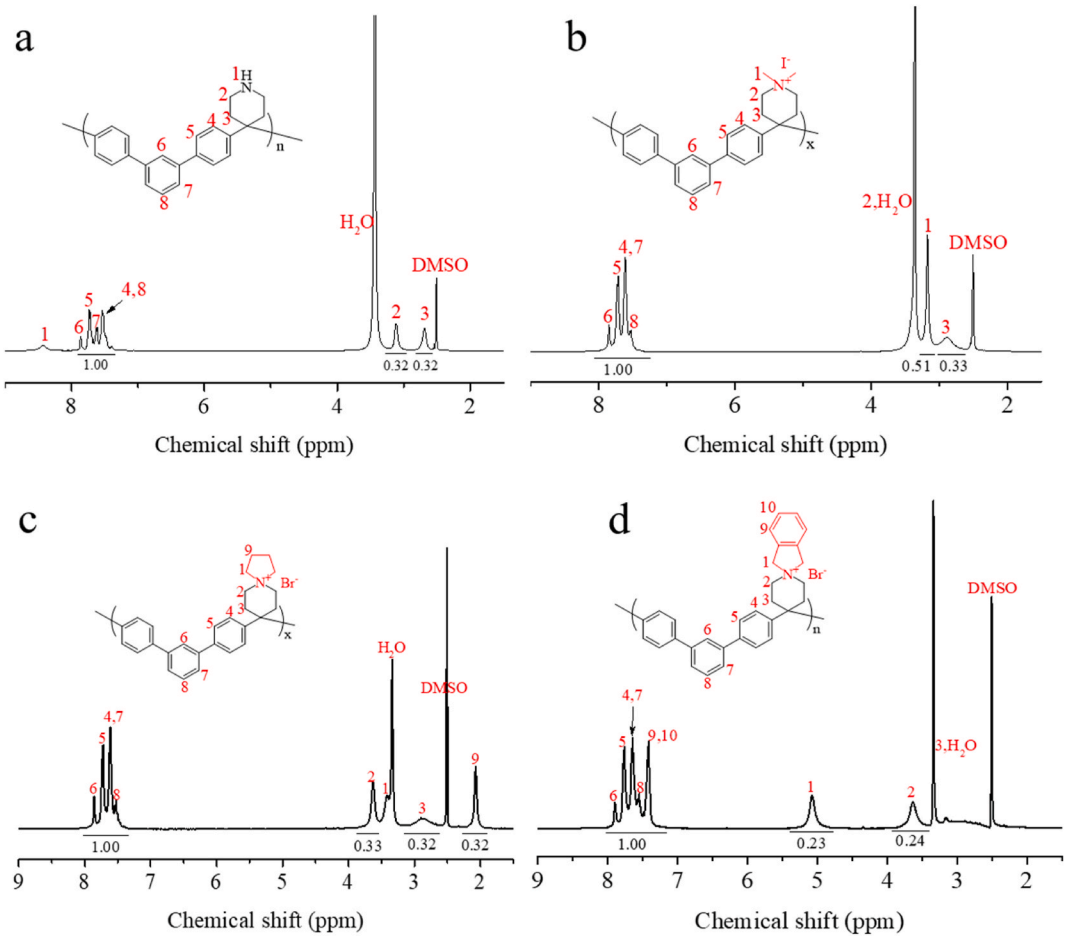

Fig. 1. ^{1}H NMR spectra of the m-TPN (a) and quaternized polymers m-TPNPiQA (b), m-TPNPyQA (c) and m-TPNBeQA (d).

for ion exchanging, then washed with DI water and dried at 60 °C for 24 h. The dried membranes were embedded in a SPI-Pon™ 812 epoxy resin, sectioned to 60 nm thickness using a microtome. Then the ultrathin film was placed on carbon-coated copper grids. Fast Fourier transformation (FFT) of the TEM images were done by ImageJ.

Small-angle X-ray scattering (SAXS). The fabricated AEMs were analyzed using the SAXS spectrometer (SAXS SYSTEM, XENOCS, France). Bragg's law was used to calculate the *d*-spacing of the AEMs.

$$d = \frac{2\pi}{q} \tag{7}$$

where the q is the location of the characteristic peak.

Alkaline stability. The alkaline stability was studied quantitatively and qualitatively by monitoring the chemical structural degradation of the AEMs in 1, 2, 5 M aq. NaOH solution at 80 °C by ^{1}H NMR spectroscopy. The NaOH solution was exchanged with fresh solution every 2 days. After 240 h, the membrane samples were taken out and washed extensively with DI water to remove any residual NaOH. Prior to the ^{1}H NMR measurements, the samples were dried for at least 24 h at 60 °C under vacuum.

Calculation of molecular orbitals. The lowest unoccupied molecular orbital (LUMO) energies of the cations was obtained by ground state density functional theory (DFT) using the B3LYP method with 6-311G++(d,p) basis set implemented in Gaussian software [34].

3. Results and discussion

3.1. Polymer synthesis and characterization

Friedel-Crafts type polycondensation was applied to synthesize ether-free precursor polymer m-TPN. The chemical structure and purity of this precursor was confirmed by ^{1}H NMR spectroscopy, as seen in Fig. 1a. The chemical shifts of the signals corresponding to the protons from benzene ring were observed at 7–8 ppm (H_4–H_8), while the peaks belonged to piperidinium moiety were located at 2.6 ppm (H_3) and 3.2 ppm (H_2). The characteristic peak of the proton (H_1) near the N atom is located at 8.56 ppm. The integral area ratio of the peaks $H_{4\text{-}8}$ and H_2 is determined to be 1:0.32 which is consistent with the theoretical value (1:0.33) in the polymer structure, indicating that m-TPN was synthesized successfully.

The corresponding functionated copolymers (m-TPNPiQA, m-TPNPyQA and m-TPNBeQA) were obtained by either cyclo-quaternized using α,α′-Dibromo-o-xylene and 1,4-dibromopentane or mono-quaternized using Iodomethane, as presented in Scheme 1. It is observed from Fig. 1b–d that the proton (–NH–) at 8.56 ppm totally disappeared while the new signals appeared for m-TPNPiQA, m-TPNPyQA and m-TPNBeQA. Besides the signals (H_4–H_8) originating from the benzene rings remained rather unchanged. For the m-TPNPiQA (Fig. 1b), the signals around 2.9 ppm and 3.2 ppm are ascribed to the proton from $–CH_3$ and $–CH_2$-, respectively. For the m-TPNPyQA (Fig. 1c), the four characteristic peaks ranged from 2.0 to 3.8 ppm are attributed to $–CH_2$- group in the cations. For the m-TPNBeQA (Fig. 1d), the new peaks (H_9, H_{10}) around 7.4 ppm are ascribed to the proton resonance from benzene ring in the cationic groups. The integral area

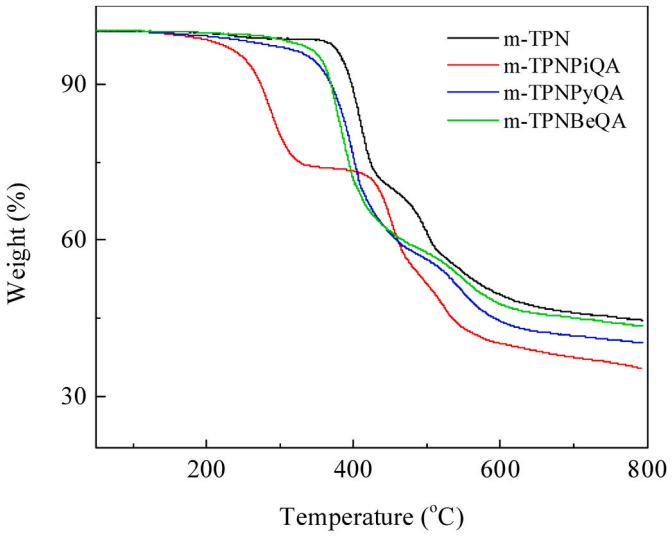

Fig. 2. TGA traces of the m-TPN, m-TPNPiQA, m-TPNPyQA and m-TPNBeQA polymers at a heating rate of 10 °C min^{-1} under nitrogen atmosphere.

ratio of the peaks is consistent with the theoretical values, indicating the designed polymers have been successfully synthesized.

This simple synthesis method provides a good possibility for scale up. The length of the polymer chains was carefully controlled by adjusting the TFSA feed. A higher molecular weight of the synthesized polymer is beneficial to improve the film-forming properties of the membranes. The number average and weight average molecular weight of precursor m-TPN (Fig. S1) were measured to be 26.6 kDa and 51.6 kDa, respectively. The polydispersity was calculated to be 1.94. This means our polymer is good enough for constructing membranes.

The TGA curves of the m-TPN, m-TPNPiQA, m-TPNPyQA and m-TPNBeQA are present in Fig. 2. There are two main thermal decompositions steps with distinct weight loss stages for the precursor polymer m-TPN. The first weight loss started around 380 °C and corresponds to the decomposition of the piperidine ring and the second weight loss starting from 440 °C is attributed to the decomposition of the rigid backbone. After functionalization, the initial thermal decomposition temperature (T_d) of the samples decreases depending on the specific cation tethered to the polymer. The T_d of the functionalized polymers (m-TPNPyQA and m-TPNBeQA) with spiro-cations are lower than the precursor but are still above 300 °C. It is also found that the piperidinium-functionalized polymer (m-TPNPiQA) with smaller cationic group starts to decompose already at 200 °C. This means the thermal stability is strongly influenced by the chemical structure of the cations. The cations with a spirocyclic structure have a significantly higher T_d than that of AEM without.

The glass transition temperatures (T_g) of the m-TPNPiQA, m-TPNPyQA and m-TPNBeQA polymers, as shown in Fig. S2, which were determined to be 190, 267 and 290 °C, respectively. The high T_g values can be explained by the highly rigid benzene backbone structure. The same backbone attached with different cationic groups (PiQA, PyQA and BeQA) show different T_g values which increase with the size of the ionic group.

3.2. Morphology

Similar to FAA-3-50, the as-prepared AEMs are transparent, uniform and smooth, as shown in Fig. 3. Besides, these AEMs can be bended, indicating the membranes are flexible enough for electrochemistry applications. The surface morphology is similar for all these AEMs with various cations in the SEM images, which indicates the homogeneous and dense AEMs are prepared successfully.

In order to achieve high conductivity, a microphase separated structure in the membranes is suggested [3,36]. It is likely that the presence of the twisted backbone would allow the polymer chain to form a compact structure and promote the self-assembly of the ionic groups [31]. Besides, the size/type of the cations could also affect the morphology of the membranes [37,38]. Herein, TEM and SAXS were applied to investigate the morphology of the as-prepared AEMs. As shows in Fig. 4a–c, the dark and bright areas refer to the hydrophilic domains and hydrophobic domains, respectively. The degree of microphase separation in m-TPNPiQA is more obvious in the TEM than for the other two AEMs (and also supported by the SAXS pattern). It is found that increasing the steric hindrance of cations go against to the degree of microphase separation. The smaller cationic groups improve ion clustering, leading to the formation of larger and more connected ion pathway channels. The reason may be that the rigidity of the cation increased with increasing steric hindrance which could be harmful to the self-assembly of the polymer chain. The phase separation behavior of

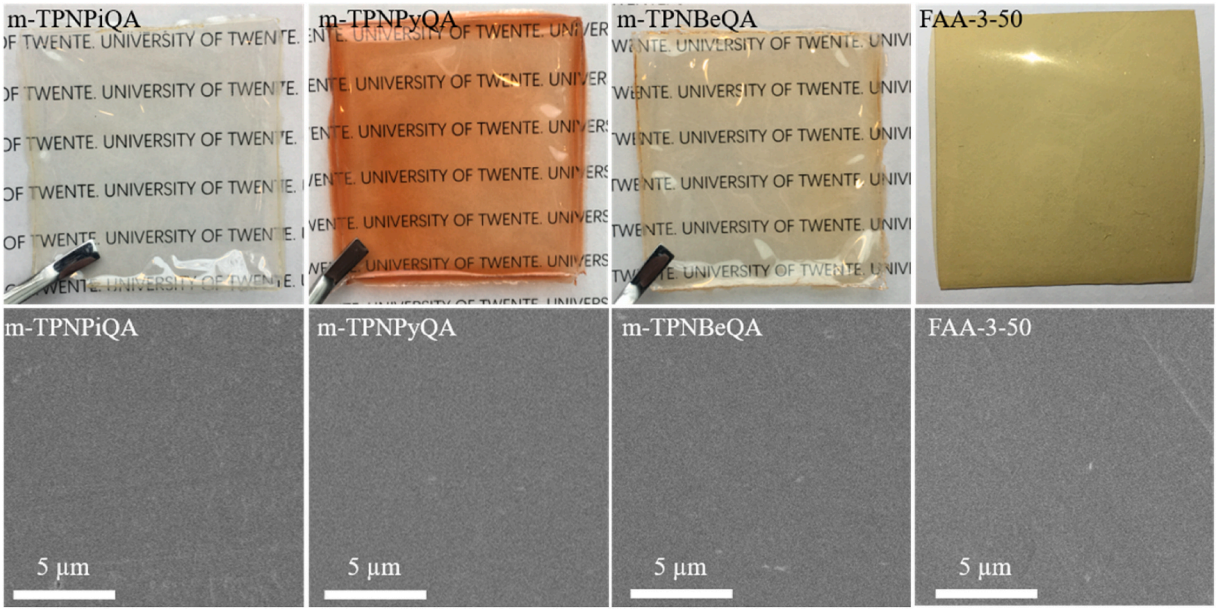

Fig. 3. Digital photos and SEM images of the AEMs.

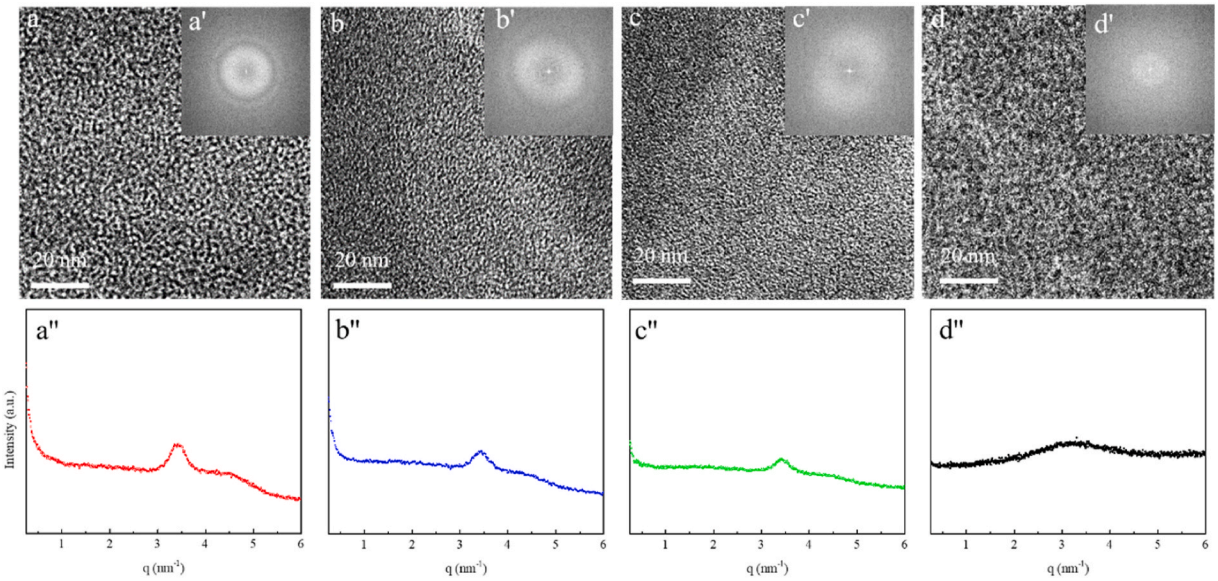

Fig. 4. TEM, FFT images and SAXS patterns for m-TPNPiQA (a,a',a''), m-TPNPyQA (b,b',b''), m-TPNBeQA (c,c',c'') and FAA-3-50.

Table 1
The IEC, WU, SR, λ and σ of the m-TPNPiQA, m-TPNPyQA and m-TPNBeQA AEMs.

Samples	IEC (meq g^{-1})		WU (%)	SR (%)	λ	σ (mS cm^{-1})
	NMR[a]	Titr[b]			20 °C	
m-TPNPiQA	2.66 (2.80)	2.54 (2.66)	52.28	21.14	10.92	22.11
m-TPNPyQA	2.49 (2.61)	2.32 (2.42)	45.12	16.15	10.36	14.94
m-TPNBeQA	2.22 (2.32)	1.99 (2.07)	30.51	12.50	8.19	12.12
FAA-3-50	–	2.02[c] (2.10)	44.00	18.21	11.06	31.20

Ionic exchange capacity (IEC), water uptake (WU) and swelling ratio (SR).
Note.
[a] Determined from ^{1}H NMR spectroscopy.
[b] Determined by titration method.
[c] Reported by Fumatech company. IEC in parentheses correspond to the values in the OH$^-$ form.

commercial membrane FAA-3-50 was different from the as-prepared AEMs due to the difference in chemical materials, where the contrast of bright domain and dark domain is less regular. This phenomenon is further visible from their corresponding FFT images (Fig. 4a'-c') which were directly transferred from the TEM images. The obvious scatter rings represent the periodic distance (*d*) of ionic segregation behavior inside the membrane. It becomes more obvious with decreasing steric hindrance of the cations. The long period of the m-TPNPiQA was approximately 1.53 nm and a weaker wider ring was also observed with *d* of 1.31 nm. A somewhat similar FFT was also shown in m-TPNPyQA with corresponding *d* observed at 1.01 nm and 0.82 nm. The m-TPNBeQA and FAA-3-50 only show a diffuse scatter ring.

Consistent results were further obtained from SAXS analysis, as shown in Fig. 4a''-c''. The difference in cationic groups slightly affects the membrane self-assembly behavior. The resulting SAXS profiles confirm the microphase separated structure formed in the membranes. For m-TPNPiQA, m-TPNPyQA, and TPNBeQA, a clear peak and a weaker peak are visible while FAA-3-50 displays a more diffuse broad peak. The main corresponding peak values fall into the range for *q* of 3.40–3.50 nm^{-1} (*d*-spacing = 1.80–1.85 nm), which is somewhat larger than the *d* from the FFT results. The intensity of the characteristic peak decreased slightly with increasing the steric hindrance of the cationic groups. These results indicate that the as-prepared AEMs with a proper arrangement of twisted ether-free polymer backbone and N-cyclic ion moieties form ion-conductive polyelectrolyte membrane with a

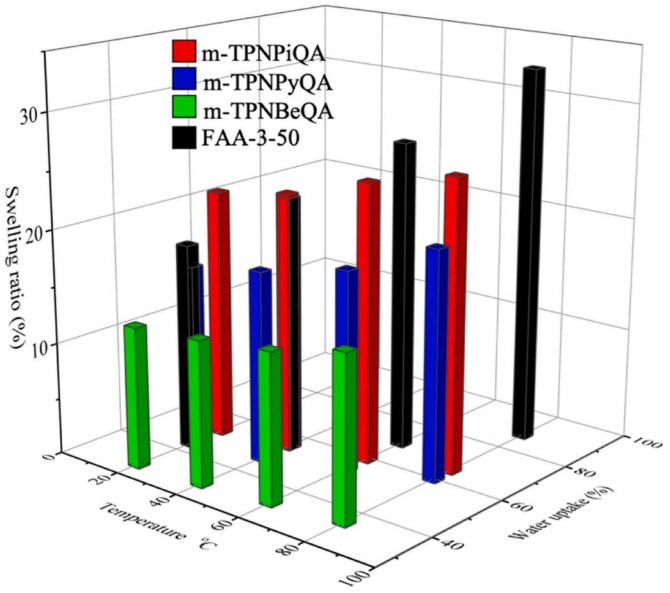

Fig. 5. Temperature dependence of WU and SR of the fully hydrated AEMs in the OH$^-$ form.

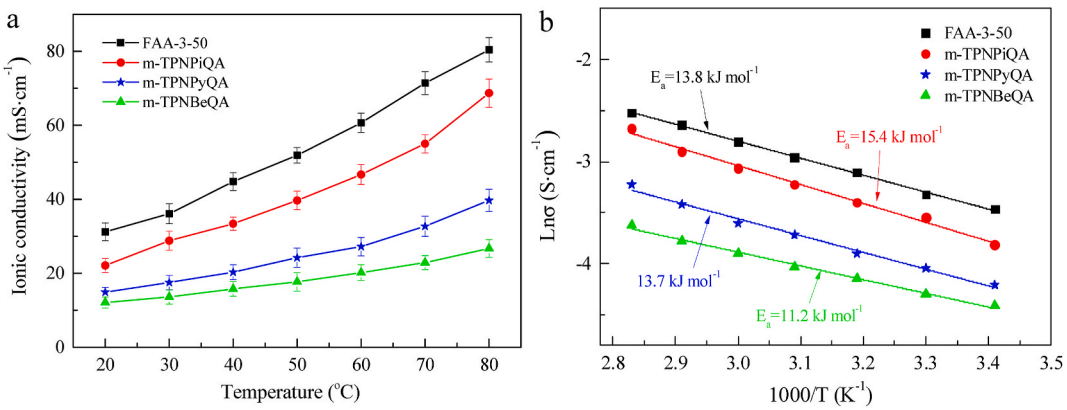

Fig. 6. Temperature dependence of hydroxide conductivities of the AEMs and their Arrhenius plots.

microphase separated structure.

As shown in Table 1, the IEC_{NMR} values of the AEMs were calculated from the corresponding NMR spectra via comparing the integration area of the signals of H_1 to H_4–H_8. It is found that the IEC_{NMR} values are in good agreement with the IEC_{titr} values in the Cl^- form obtained by titration. As seen, the IEC_{NMR} of m-TPNPiQA, m-TPNPyQA and m-TPNBeQA were 2.66, 2.49 and 2.22 meq g^{-1}, respectively, while their corresponding titration values were 2.54, 2.32 and 1.99 meq g^{-1}, respectively. The IEC_{OH^-} was calculated based on the IEC in Cl^- form, where the values were a bit higher due to a smaller molecular weight of OH^- than Cl^-. The IEC decreased with increasing size of cationic group.

The presence of water is essential for ion transportation in the membranes. However, an excess of water will result in a poor mechanical stability of the AEMs and dilution of ion concentration. Table 1 and Fig. 5 shows the WU and SR of the AEMs. The WU of the membranes slightly increases with increasing temperature because the mobility of the polymer chains increases at elevated temperature enhancing water absorption. The m-TPNPiQA with the highest IEC_{OH^-} (2.66 meq g^{-1}) exhibits the highest WU of 52.3% and 65.1% at 20 °C and 80 °C, respectively, while m-TPNBeQA has the lowest WU (30.5–35.2% at 20–80 °C) due to its lower IEC and rigid structure. It should be noted that the WU of the as-prepared AEMs doesn't change a lot at elevated temperatures while the FAA-3-50 membrane increased twofold from 44.0% to 88.0%. This may be ascribed to the hydrophobic rigid backbone of the AEMs. Fig. 5 also shows the swelling ratio of the AEMs. In spite of a higher SR at 20 °C, the m-TPNBeQA membrane have a lower SR (25.7%) than that of FAA-3-50 (33.0%) at elevated temperature (80 °C). This indicates our membranes possess excellent reduced swelling characteristics. Moreover, we found that the size of the cationic group affects the WU and SR of the AEMs. The m-TPNPiQA membrane with the smaller cation shows a higher WU and SR than that of the m-TPNPyQA and m-TPNBeQA membranes with the bulky spirocyclic QA groups. This is also in line with the surface wettability of the membranes which is further measured by the water contact angle measurement. As shown in Fig. S3. The m-TPNPiQA membrane shows the lowest contact angle at 74° because of its small steric hindrance and reduced rigidity, while the m-TPNPyQA (79.8°) and m-TPNBeQA (84.3°) membranes have higher contact angles.

3.3. Conductivity

The ionic conductivity of an AEM is an important parameter regarding the output power of energy conversion devices. Fig. 6a shows the hydroxide ion conductivity of the AEMs as a function of temperature. The conductivity increased with increasing temperature as expected. For the as-prepared AEMs, the conductivity of m-TPNPiQA membrane can reach up to 22.1–68.7 mS cm^{-1} at 20–80 °C caused by the smaller charge groups that result in slightly higher water uptake. The m-TPNPyQA and m-TPNBeQA membranes with a larger steric effect exhibit conductivities of 14.9–39.7 mS cm^{-1} and 12.1–26.7 mS cm^{-1}, respectively. The difference in morphology also supports their ion conductivity, as m-TPNPyQA and m-TPNBeQA display reduced microphase separation. The m-TPNPiQA membrane has the most obvious microphase separated morphology which can form the efficient pathway for ion conduction. The conductivity of the m-TPNPiQA membrane is very close to that of the commercialized FAA-3-50 membrane (31.2–80.4 mS cm^{-1}, 20–80 °C), confirming their potential for practical applications. However, the conductivity of m-TPNPiQA is lower than that of reported poly

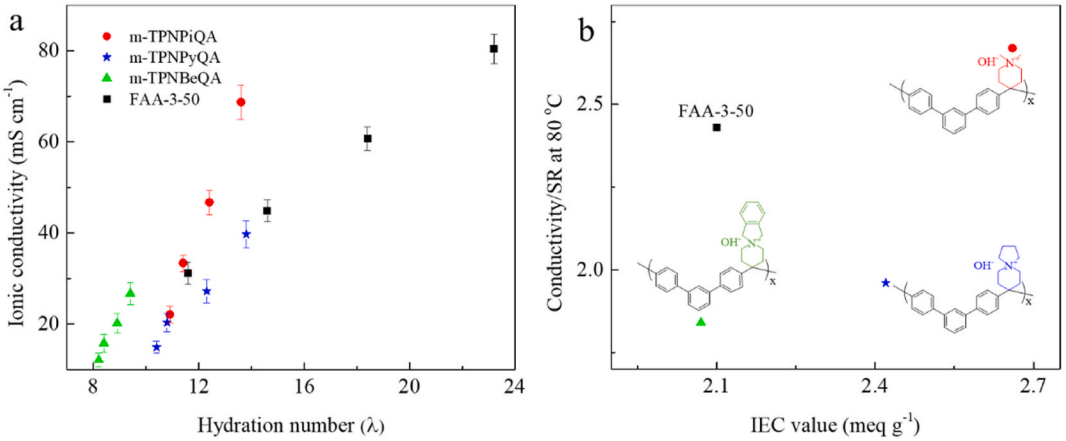

Fig. 7. (a) Ionic conductivity of the AEMs as a function of hydration number and (b) the conductivity/SR versus IEC.

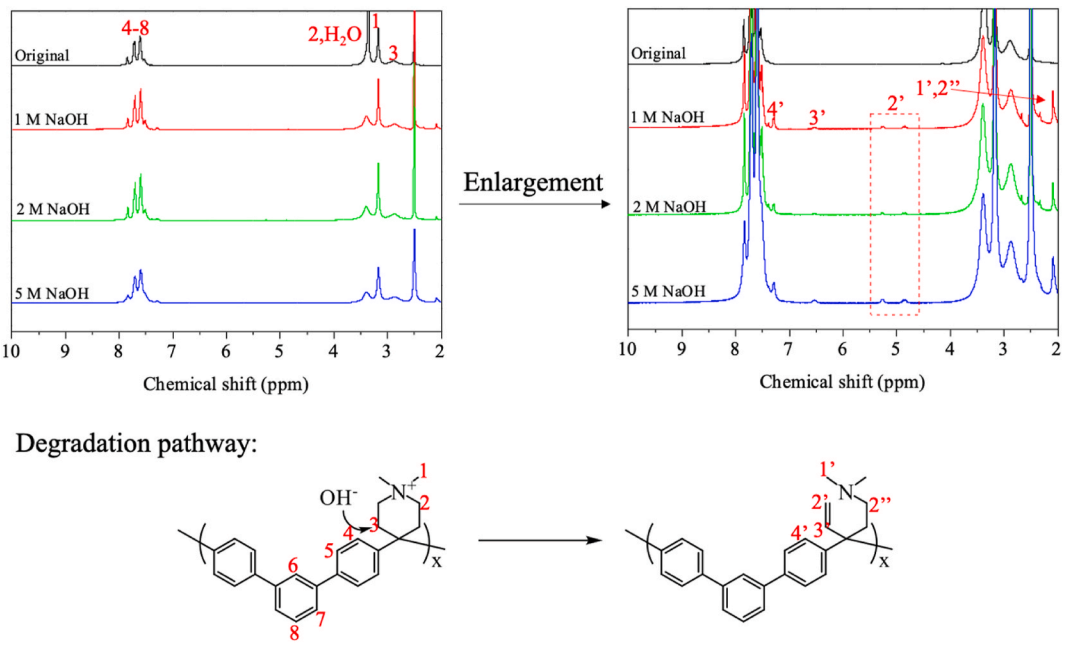

Fig. 8. Alkaline stability test results of the m-TPNPiQA and the proposed degradation mechanism.

(terphenylene)-based AEMs with alkyl quaternary ammonium since the cationic groups of m-TPNPiQA is close to the backbone which could restrict the local mobility of the ionic groups [31]. The transport activation energies (E_a) for all AEMs are ranged from 11.2 to 15.4 kJ mol^{-1} (Fig. 6b), and these results are comparable to reported AEMs [8,39–41].

Basically, the membrane with high IEC and WU improves the ion transportation, but an excess of WU and consequently SR dilutes the ion concentration and result in a poor conductivity. One of the major challenges is to develop AEMs with high ionic conductivity combined with a low SR, thus a relatively low hydration number λ. Fig. 7a shows the relation between the ion conductivity and hydration number for each membrane. The as-prepared AEMs exhibits a lower hydroxide conductivity for a given temperature ((20, 40, 60 and 80 °C), combined with lower λ values than those of commercial FAA-3-50. Besides, we introduce the conductivity against SR (σ/SR) to evaluate the performance of the AEMs, as shown in Fig. 7b. An important finding of this work is that the m-TPNPiQA membrane has a higher σ/SR than that of FAA-3-50 membrane. The twisted rigid backbone of the as-prepared AEMs resists swelling and provides a better balance of WU and conductivity.

3.4. Alkaline stability

Long-term stability of the AEMs in alkaline environment concerns a challenge for the development of membrane materials for energy conversion devices. Under alkaline condition, the cationic groups and backbones are vulnerable to the hydroxide ions at elevated temperature, leading to the degradation of the AEMs. Herein, the N-cyclic QA cations can potentially degrade via Hofmann elimination and/or direct nucleophilic substitution reaction under these high pH condition. In order to investigate the chemical stability of the as-prepared AEMs with various cationic groups, the membrane materials were treated in NaOH solution with different concentration (1, 2 and 5 M) at 80 °C for 240 h.

The m-TPNPiQA showed signs of slight degradation confirmed by the appearance of new signals (H_1'-H_4', H_2″) and a decline in the intensity of –CH_3 groups (H_1) close to the N atom, as shown in Fig. 8. By comparing the integral areas of H_1 to H_4–H_8, it is found that the degradation becomes more severe with increasing concentration of NaOH solution. The ratio of integral area for the new peaks at 6.5, 5.2 and 4.8 ppm are equal to 1:1:1. This is also in accordance with the formation of alkenyl protons (CH_2═CH- group), indicating the ring-opening β-elimination reaction occurred during this stability test. The new peaks around 2.1 ppm and 7.3 ppm correspond to the degradation product. The proposed degradation pathway of m-TPNPyQA is presented in Fig. 8. The AEMs degradation causes cationic loss leading to decreased IEC. As reported in Table 2, the IEC_{NMR} of m-TPNPiQA decreased to 97.4%, 97.0% and 94.0% of the initial values after treating with 1 M, 2 M and 5 M NaOH solution, respectively, indicating the AEMs with piperidinium groups and ether-bond free backbone are quite stable under alkaline condition. For comparison, the conductivity of conventional quaternized PPO-based AEM with ether-bond degraded by appr. 60% and was broken into small pieces after treatment in 1 M NaOH at 80 °C for 80 h [42]. Besides, the chemical stability of m-TPNPiQA is similar to the reported AEMs with an ether-bond free backbone and alkyl quaternary ammonium. As reported, the IEC of a $PBPA^+$ membrane decreased to 99.6% after an alkaline test in 1 M NaOH solution at 80 °C for 30 days [43].

The m-TPNPyQA showed signs of degradation as confirmed by the appearance of new signals (marked by red circle) and a decline in intensity of the –CH_2- groups close to the N atom, as shown in Fig. 9. These new peaks were barely detected after exposure to the 1 M NaOH solution, but are apparent in the 2 M and 5 M NaOH solution. The ratio of integral area for those new peaks (H_2' and H_3') at 6.5, 5.2 and 4.8 ppm are equal to 1:1:1. This is in accordance with the formation of alkenyl protons (CH_2═CH- group), consistent with the ring-opening

Table 2
The IEC_{NMR} of the AEMs before and after immersing in 1, 2 and 5 M NaOH solution at 80 °C for 240 h.

Samples	Original IEC (meq g^{-1})	1 M (meq g^{-1})	2 M (meq g^{-1})	5 M (meq g^{-1})
m-TPNPiQA	2.66	2.59	2.58	2.50
m-TPNPyQA	2.49	2.28	2.10	2.03
m-TPNBeQA	2.22	1.59	1.54	1.24

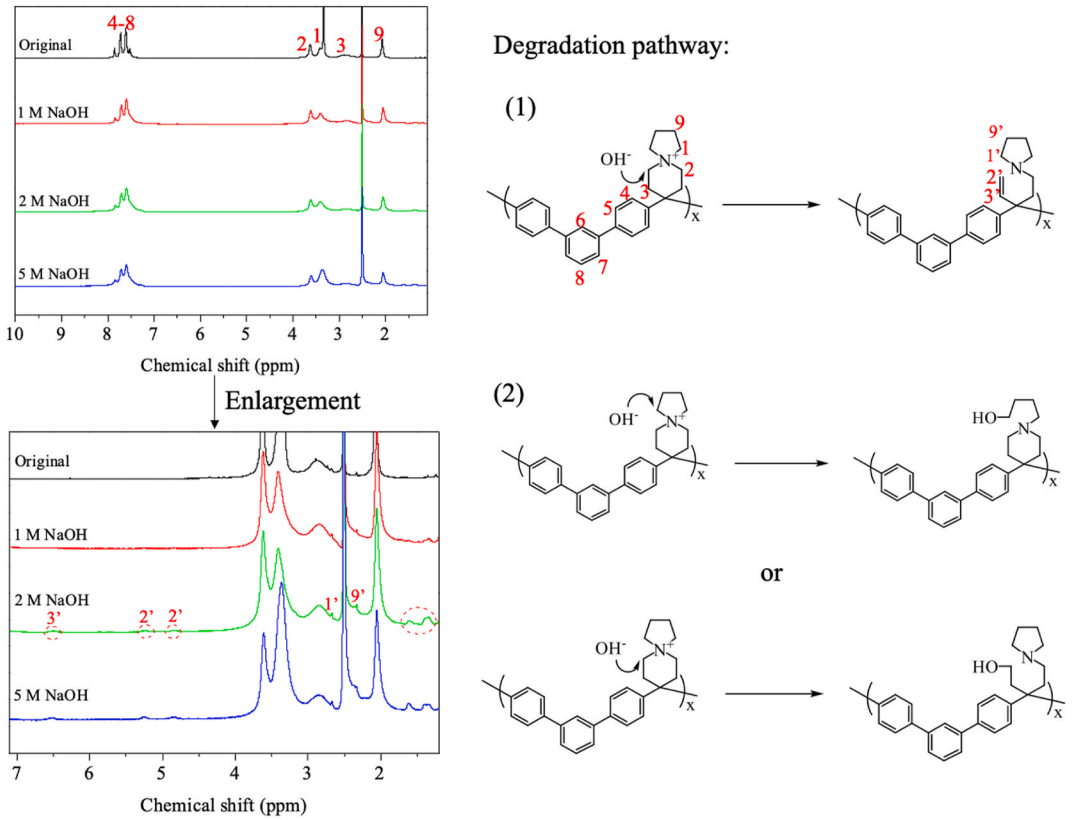

Fig. 9. ^{1}H NMR spectra of the m-TPNPyQA before and after alkaline stability test and the proposed degradation mechanism.

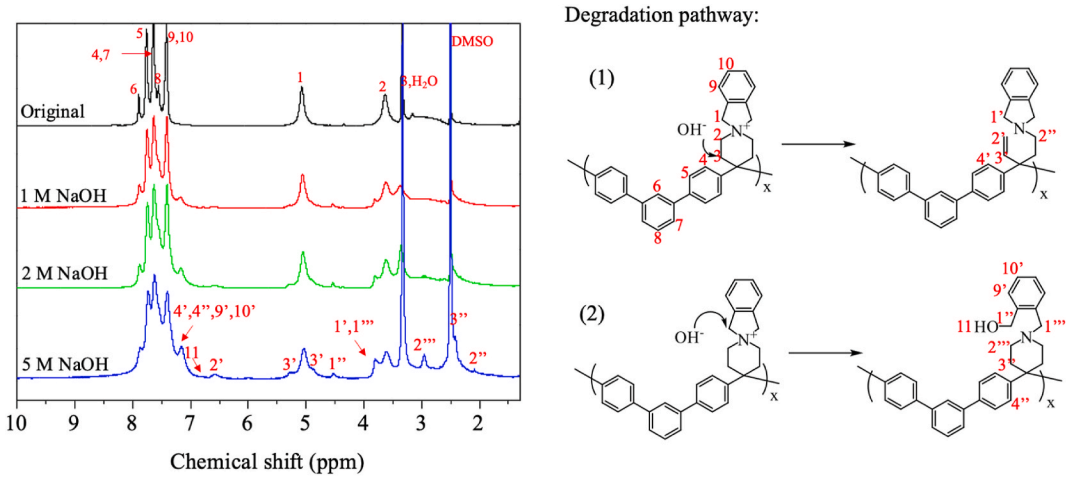

Fig. 10. ^{1}H NMR spectra of the m-TPNBeQA before and after alkaline stability test and the proposed degradation mechanism.

β-elimination. Except for the β-elimination, the AEMs can also degrade by the nucleophilic substitution reaction. New signals were also observed at 1.4 and 1.6 ppm, which may be attributed to the degradation product of the cations via nucleophilic substitution reaction. By comparing the integral area of the protons from the $-CH_2-$ group to the protons from the benzene rings, the degradation degree can be quantified. The IEC_{NMR} of m-TPNPyQA (Table 2) decreased to 91.6%, 84.3% and 81.5% of the initial values after treating with 1 M, 2 M and 5 M NaOH solution, respectively. Combined with the results of Pham et al. [20], the proposed degradation pathways of m-TPNPyQA are presented in Fig. 9. The reduced alkaline stability of the AEMs with N-spirocyclic QA cations is most probably attributed to the distortion of the piperidinium ring conformation by the rigid poly(terphenylene) backbone. Attaching the piperidine rings directly to the rigid backbone may significantly distort the bond angles and constrain conformational relaxation for the N-spirocyclic QA cations, thus decreasing the activation energy and promoting the degradation reactions [20]. As a result, the m-TPNPyQA membranes were more susceptible to β-elimination compared to m-TPNPiQA.

For the m-TPNBeQA, the degradation signals were also observed in the ^{1}H NMR spectra (Fig. 10). The OH^{-} ion may attack the α-C atom resulting in the degradation of cations. Here, the new signals from the alkenyl protons ($CH_2{=}CH-$ group) were also observed (H_2' and H_3'), indicating the ring-opening β-elimination reaction occurred during stability test. As noted by Lin et al. and Chu et al. [9,44], the proposed degradation mechanism is present in Fig. 10. The nucleophilic

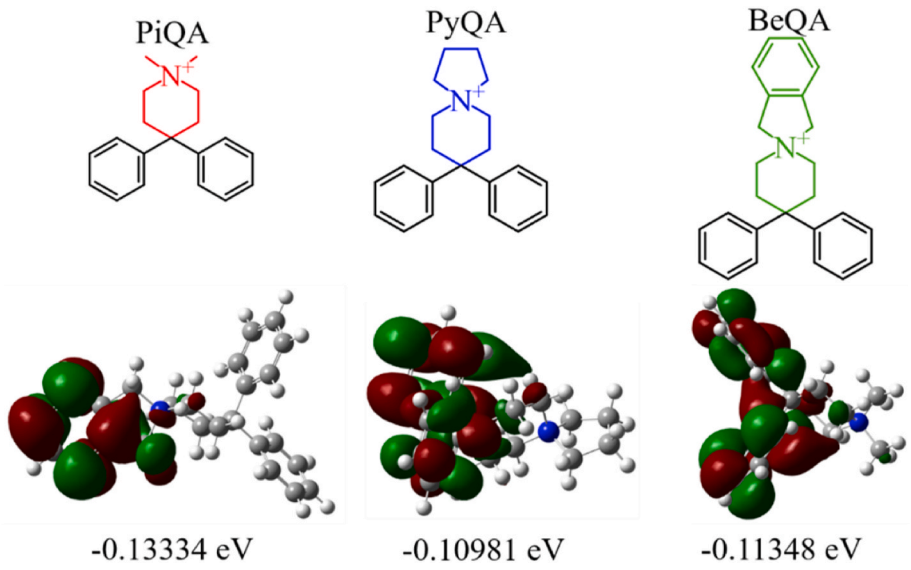

Fig. 11. Molecular structures and LUMO iso-surfaces of model molecules.

substitution reaction happened in m-TPNBeQA, where new peaks (H_1'', H_1''', H_3'', H_4'', H_9', H_{10}', H_{11}) are ascribed to the degradation products of the cation. By comparing the integral area of –N(CH_2)- with benzene rings (H_4–H_8) in the backbone, the IEC_{NMR} of m-TPNBeQA (Table 2) decreased to 71.2%, 69.4% and 55.8% of the initial values after treating with 1 M, 2 M and 5 M NaOH solution, respectively.

No apparent change in the ^{1}H NMR signals was observed for the backbones of the as-prepared AEMs, and the membrane materials retained appearance and flexibility after stability test, confirming the excellent alkaline stability of the ether-free backbone. However, it seems that the bulky benzene ring cannot protect the N-spirocyclic quaternary ammonium group from degradation. The order of chemical stability in concentrated NaOH was m-TPNPiQA > m-TPNPyQA > m-TPNBeQA. m-TPNBeQA with the largest cation undergoes significant degradation, while m-TPNPiQA with the smallest cation has the best alkali resistance among the membranes. The results show that more durable AEMs can be achieved by tuning the cation structure.

In general, a lower LUMO energy allows the OH^- to attack the cationic groups more easily and results in a poorer chemical stability of the cations [35,45]. The LUMO energies of the model cations PiQA, PyQA, and BeQA were calculated to be −0.13334, −0.10981 and −0.11348 eV, respectively, as shown in Fig. 11. The LUMO energy of PyQA is higher than that of BeQA, suggesting that PyQA exhibits better alkaline stability compared to BeQA. This phenomenon is consistent with the above results that the corresponding m-TPNBeQA degrades more severely than m-TPNPyQA. Although the LUMO energy of PiQA is lower than other two cations, our NMR results demonstrated that the corresponding m-TPNPiQA AEM is actually more stable than other two AEMs. The practical stability of the cations tethered to backbone is also affected by the backbone structure and morphology of the AEMs. Since the corresponding AEMs have the same backbone, the reason for the difference between the AEMs can be explained by the difference in morphology. The stronger hydrophilic/hydrophobic phase separated structure may favor the alkaline stability of m-TPNPiQA since the OH^- can be well-solvated in the hydrophilic environment and leads to a slower chemical reaction between cationic groups and OH^- [46,47]. Similar phenomenon can be found in the literature [48]. The reduced alkaline stability of the AEMs with spirocyclic cations may be partly caused by the lower water uptake and λ values since this will increase the concentration of the harmful hydroxide ions [32,49].

4. Conclusions

In summary, a series of poly(terphenylene)-based AEMs with various N-cyclic cations were systematically prepared to understand the role of N-cyclic cationic groups on the membrane overall performance. Incorporation of twisted ether-bond free backbone and N-cyclic cations results in a relative high conductivity and robust alkaline stability. The m-TPNPiQA exhibited the highest conductivity due to the obvious microphase separation structure formed inside the membrane. However, increasing the steric hindrance of cation constrains the water absorption and reduces dimensional swelling at the expense of reduced ion conductivity. Compared to the commercial FAA-3-50 membrane, the as-prepared AEMs have relatively high ionic conductivity. Furthermore, the ether-free poly(terphenylene) chain enables a stable backbone under alkaline condition, while the N-cyclic cations of the AEMs are found to degrade via β-Hofmann elimination and/or nucleophilic substitution reaction. The degradation of the cations become more severe by increasing the size of cations since the distortion of the piperidinium ring conformation by the rigid poly(terphenylene) backbone could decrease the stability of cations. The presented material properties and characteristics confirm their potential for relevant applications in alkaline fuel cell and electrolysis processes.

CRediT authorship contribution statement

Xiuqin Wang: Conceptualization, Methodology, Validation, Formal analysis, Investigation, Resources, Writing – original draft, Writing – review & editing. **Chenxiao Lin:** Formal analysis, Resources, Writing – review & editing. **Yang Gao:** Formal analysis, Resources, Writing – review & editing. **Rob G.H. Lammertink:** Writing – review & editing, Supervision.

Declaration of competing interest

The authors declare the following financial interests/personal relationships which may be considered as potential competing interests: There are no conflicts to declare.

Lammertink reports financial support was provided by Netherlands Organisation for Scientific Research (NWO). Wang reports financial support was provided by China Scholarship Council. Lin reports financial support was provided by Guangdong Basic and Applied Basic Research Fund.

Acknowledgments

Financial support from the Guangdong Basic and Applied Basic Research Fund (2019A1515111188) and China Scholarship Council (CSC) are gratefully acknowledged. This work is part of the Vici project STW 016.160.312 which is financed by the Netherlands Organisation for Scientific Research (NWO).

Appendix A. Supplementary data

Supplementary data to this article can be found online at https://doi.org/10.1016/j.memsci.2021.119525.

References

[1] L. Wang, X. Peng, W.E. Mustain, J.R. Varcoe, Radiation-grafted anion-exchange membranes: the switch from low- to high-density polyethylene leads to remarkably enhanced fuel cell performance, Energy Environ. Sci. 12 (2019) 1575–1579.
[2] X. Peng, T.J. Omasta, E. Magliocca, L. Wang, J.R. Varcoe, W.E. Mustain, Nitrogen-doped carbon–CoO_x nanohybrids: a precious metal free cathode that exceeds 1.0 W cm^{-2} peak power and 100 h life in anion-exchange membrane fuel cells, Angew. Chem. Int. Ed. 58 (2019) 1046–1051.
[3] J.R. Varcoe, P. Atanassov, D.R. Dekel, A.M. Herring, M.A. Hickner, P.A. Kohl, A. R. Kucernak, W.E. Mustain, K. Nijmeijer, K. Scott, Anion-exchange membranes in electrochemical energy systems, Energy Environ. Sci. 7 (2014) 3135–3191.
[4] C.X. Lin, X.L. Huang, D. Guo, Q.G. Zhang, A.M. Zhu, M.L. Ye, Q.L. Liu, Side-chain-type anion exchange membranes bearing pendant quaternary ammonium groups via flexible spacers for fuel cells, J. Mater. Chem. 4 (2016) 13938–13948.
[5] C. Lin, Y. Gao, N. Li, M. Zhang, J. Luo, Y. Deng, L. Ling, Y. Zhang, F. Cheng, S. Zhang, Quaternized Tröger's base polymer with crown ether unit for alkaline stable anion exchange membranes, Electrochim. Acta 354 (2020) 136693.
[6] Z. Li, G. He, Z. Li, Y. Zhang, J. Zhao, M. Xu, S. Xu, Z. Jiang, Enhancing the hydroxide conductivity of imidazolium-functionalized polysulfone by incorporating organic microsphere with ionic brushes, J. Membr. Sci. 554 (2018) 6–15.
[7] Y. Wang, D. Zhang, X. Liang, M.A. Shehzad, X. Xiao, Y. Zhu, X. Ge, J. Zhang, Z. Ge, L. Wu, T. Xu, Improving fuel cell performance of an anion exchange membrane by terminal pending bis-cations on a flexible side chain, J. Membr. Sci. 595 (2020) 117483.
[8] C. Lin, J. Wang, G. Shen, J. Duan, D. Xie, F. Cheng, Y. Zhang, S. Zhang, Construction of crosslinked polybenzimidazole-based anion exchange membranes with ether-bond-free backbone, J. Membr. Sci. 590 (2019) 117303.
[9] C. Lin, D. Yu, J. Wang, Y. Zhang, D. Xie, F. Cheng, S. Zhang, Facile construction of poly(arylene ether)s-based anion exchange membranes bearing pendent N-spirocyclic quaternary ammonium for fuel cells, Int. J. Hydrogen Energy 44 (2019) 26565–26576.
[10] J.S. Olsson, T.H. Pham, P. Jannasch, Functionalizing polystyrene with N-alicyclic piperidine-based cations via Friedel–Crafts alkylation for highly alkali-stable anion-exchange membranes, Macromolecules 53 (2020) 4722–4732.
[11] X. Zhang, X. Chu, M. Zhang, M. Zhu, Y. Huang, Y. Wang, L. Liu, N. Li, Molecularly designed, solvent processable tetraalkylammonium-functionalized fluoropolyolefin for durable anion exchange membrane fuel cells, J. Membr. Sci. 574 (2019) 212–221.
[12] H.-S. Dang, E.A. Weiber, P. Jannasch, Poly (phenylene oxide) functionalized with quaternary ammonium groups via flexible alkyl spacers for high-performance anion exchange membranes, J. Mater. Chem. 3 (2015) 5280–5284.
[13] M. Marino, K. Kreuer, Alkaline stability of quaternary ammonium cations for alkaline fuel cell membranes and ionic liquids, ChemSusChem 8 (2015) 513–523.
[14] K. Yang, X. Chu, X. Zhang, X. Li, J. Zheng, S. Li, N. Li, T.A. Sherazi, S. Zhang, The effect of polymer backbones and cation functional groups on properties of anion exchange membranes for fuel cells, J. Membr. Sci. 603 (2020) 118025.
[15] B. Xue, Q. Wang, J. Zheng, S. Li, S. Zhang, Bi-guanidinium-based crosslinked anion exchange membranes: synthesis, characterization, and properties, J. Membr. Sci. 601 (2020) 117923.
[16] B. Zhang, S. Gu, J. Wang, Y. Liu, A.M. Herring, Y. Yan, Tertiary sulfonium as a cationic functional group for hydroxide exchange membranes, RSC Adv. 2 (2012) 12683–12685.
[17] X. Yan, S. Gu, G. He, X. Wu, W. Zheng, X. Ruan, Quaternary phosphonium-functionalized poly(ether ether ketone) as highly conductive and alkali-stable hydroxide exchange membrane for fuel cells, J. Membr. Sci. 466 (2014) 220–228.
[18] M.T. Kwasny, L. Zhu, M.A. Hickner, G.N. Tew, Thermodynamics of counterion release is critical for anion exchange membrane conductivity, J. Am. Chem. Soc. 140 (2018) 7961–7969.
[19] H.-S. Dang, P. Jannasch, Alkali-stable and highly anion conducting poly(phenylene oxide)s carrying quaternary piperidinium cations, J. Mater. Chem. 4 (2016) 11924–11938.
[20] T.H. Pham, J.S. Olsson, P. Jannasch, Poly(arylene alkylene)s with pendant N-spirocyclic quaternary ammonium cations for anion exchange membranes, J. Mater. Chem. 6 (2018) 16537–16547.
[21] T.H. Pham, J.S. Olsson, P. Jannasch, N-spirocyclic quaternary ammonium ionenes for anion-exchange membranes, J. Am. Chem. Soc. 139 (2017) 2888–2891.
[22] O.J. S, P.T. Huong, J. Patric, Poly(arylene piperidinium) hydroxide ion exchange membranes: synthesis, alkaline stability, and conductivity, Adv. Funct. Mater. 28 (2018) 1702758.
[23] T.H. Pham, P. Jannasch, Aromatic polymers incorporating bis-N-spirocyclic quaternary ammonium moieties for anion-exchange membranes, ACS Macro Lett. 4 (2015) 1370–1375.
[24] A. Allushi, T.H. Pham, J.S. Olsson, P. Jannasch, Ether-free polyfluorenes tethered with quinuclidinium cations as hydroxide exchange membranes, J. Mater. Chem. 7 (2019) 27164–27174.
[25] S. Li, H. Zhang, K. Wang, F. Yang, Y. Han, Y. Sun, J. Pang, Z. Jiang, Micro-block versus random quaternized poly(arylene ether sulfones) with highly dense quaternization units for anion exchange membranes, Polym. Chem. 11 (2020) 2399–2407.
[26] C.X. Lin, X.Q. Wang, L. Li, F.H. Liu, Q.G. Zhang, A.M. Zhu, Q.L. Liu, Triblock copolymer anion exchange membranes bearing alkyl-tethered cycloaliphatic quaternary ammonium-head-groups for fuel cells, J. Power Sources 365 (2017) 282–292.
[27] S. Li, H. Zhang, K. Wang, F. Yang, Y. Han, Y. Sun, J. Pang, Z. Jiang, Anion conductive piperidinium based poly (ether sulfone): synthesis, properties and cell performance, J. Membr. Sci. 594 (2020) 117471.
[28] E.A. Weiber, P. Jannasch, Anion-conducting polysulfone membranes containing hexa-imidazolium functionalized biphenyl units, J. Membr. Sci. 520 (2016) 425–433.
[29] C.G. Arges, V. Ramani, Two-dimensional NMR spectroscopy reveals cation-triggered backbone degradation in polysulfone-based anion exchange membranes, Proc. Natl. Acad. Sci. Unit. States Am. 110 (2013) 2490–2495.
[30] J. Wang, Y. Zhao, B.P. Setzler, S. Rojas-Carbonell, C. Ben Yehuda, A. Amel, M. Page, L. Wang, K. Hu, L. Shi, S. Gottesfeld, B. Xu, Y. Yan, Poly(aryl piperidinium) membranes and ionomers for hydroxide exchange membrane fuel cells, Nat. Energy 4 (2019) 392–398.
[31] W.-H. Lee, E.J. Park, J. Han, D.W. Shin, Y.S. Kim, C. Bae, Poly(terphenylene) anion exchange membranes: the effect of backbone structure on morphology and membrane property, ACS Macro Lett. 6 (2017) 566–570.
[32] T.H. Pham, J.S. Olsson, P. Jannasch, Effects of the N-alicyclic cation and backbone structures on the performance of poly(terphenyl)-based hydroxide exchange membranes, J. Mater. Chem. 7 (2019) 15895–15906.
[33] J.S. Olsson, T.H. Pham, P. Jannasch, Tuning poly(arylene piperidinium) anion-exchange membranes by copolymerization, partial quaternization and crosslinking, J. Membr. Sci. 578 (2019) 183–195.
[34] F. Wang, Y. Li, C. Li, H. Zhu, Preparation and study of spirocyclic cationic side chain functionalized polybiphenyl piperidine anion exchange membrane, J. Membr. Sci. 620 (2021) 118919.
[35] K. Matsuyama, H. Ohashi, S. Miyanishi, H. Ushiyama, T. Yamaguchi, Quantum chemical approach for highly durable anion exchange groups in solid-state alkaline fuel cells, RSC Adv. 6 (2016) 36269–36272.
[36] D.W. Shin, M.D. Guiver, Y.M. Lee, Hydrocarbon-based polymer electrolyte membranes: importance of morphology on ion transport and membrane stability, Chem. Rev. 117 (2017) 4759–4805.
[37] Y. Xing, K. Geng, X. Chu, C. Wang, L. Liu, N. Li, Chemically stable anion exchange membranes based on C2-Protected imidazolium cations for vanadium flow battery, J. Membr. Sci. 618 (2021) 118696.
[38] F.H. Liu, C.X. Lin, E.N. Hu, Q. Yang, Q.G. Zhang, A.M. Zhu, Q.L. Liu, Anion exchange membranes with well-developed conductive channels: effect of the functional groups, J. Membr. Sci. 564 (2018) 298–307.
[39] Y. Zhang, W. Chen, X. Yan, F. Zhang, X. Wang, X. Wu, B. Pang, J. Wang, G. He, Ether spaced N-spirocyclic quaternary ammonium functionalized crosslinked polysulfone for high alkaline stable anion exchange membranes, J. Membr. Sci. 598 (2020) 117650.
[40] X. Zhang, Y. Cao, M. Zhang, Y. Wang, H. Tang, N. Li, Olefin metathesis-crosslinked, bulky imidazolium-based anion exchange membranes with excellent base stability and mechanical properties, J. Membr. Sci. 598 (2020) 117793.
[41] C.X. Lin, Y.Z. Zhuo, E.N. Hu, Q.G. Zhang, A.M. Zhu, Q.L. Liu, Crosslinked side-chain-type anion exchange membranes with enhanced conductivity and dimensional stability, J. Membr. Sci. 539 (2017) 24–33.
[42] N.W. Li, T.Z. Yan, Z. Li, T. Thurn-Albrecht, W.H. Binder, Comb-shaped polymers to enhance hydroxide transport in anion exchange membranes, Energy Environ. Sci. 5 (2012) 7888–7892.
[43] W.-H. Lee, Y.S. Kim, C. Bae, Robust hydroxide ion conducting poly (biphenyl alkylene) s for alkaline fuel cell membranes, ACS Macro Lett. 4 (2015) 814–818.
[44] X. Chu, L. Liu, Y. Huang, M.D. Guiver, N. Li, Practical implementation of bis-six-membered N-cyclic quaternary ammonium cations in advanced anion exchange

membranes for fuel cells: synthesis and durability, J. Membr. Sci. 578 (2019) 239–250.
[45] Z. Si, L. Qiu, H. Dong, F. Gu, Y. Li, F. Yan, Effects of substituents and substitution positions on alkaline stability of imidazolium cations and their corresponding anion-exchange membranes, ACS Appl. Mater. Interfaces 6 (2014) 4346–4355.
[46] S. Chempath, B.R. Einsla, L.R. Pratt, C.S. Macomber, J.M. Boncella, J.A. Rau, B. S. Pivovar, Mechanism of tetraalkylammonium headgroup degradation in alkaline fuel cell membranes, J. Phys. Chem. C 112 (2008) 3179–3182.
[47] Y.Z. Zhuo, A.L. Lai, Q.G. Zhang, A.M. Zhu, M.L. Ye, Q.L. Liu, Enhancement of hydroxide conductivity by grafting flexible pendant imidazolium groups into poly (arylene ether sulfone) as anion exchange membranes, J. Mater. Chem. 3 (2015) 18105–18114.
[48] X. Yan, R. Deng, Y. Pan, X. Xu, I. El Hamouti, X. Ruan, X. Wu, C. Hao, G. He, Improvement of alkaline stability for hydroxide exchange membranes by the interactions between strongly polar nitrile groups and functional cations, J. Membr. Sci. 533 (2017) 121–129.
[49] D.R. Dekel, M. Amar, S. Willdorf, M. Kosa, S. Dhara, C.E. Diesendruck, Effect of water on the stability of quaternary ammonium groups for anion exchange membrane fuel cell applications, Chem. Mater. 29 (2017) 4425–4431.